Macromolecules

ARTICLE

pubs.acs.org/Macromolecules

Linking Network Microstructure to Macroscopic Properties of Siloxane Elastomers Using Combined Nuclear Magnetic Resonance and Mesoscale Computational Modeling

Brian P. Mayer,* James P. Lewicki, Todd H. Weisgraber, Ward Small, Sarah C. Chinn, and Robert S. Maxwell

Lawrence Livermore National Laboratory, 7000 East Avenue, Livermore, California 94550, United States

ABSTRACT: It is well established that many fundamental properties of polymer materials are directly governed by chain dynamics, and both experimental and computational efforts to probe this motional spectrum have been manifold. Recently, multiple quantum (MQ) nuclear magnetic resonance (NMR) has afforded the capability to extract meaningful quantities from such measurements, namely, an effective molecular weight distribution between various topological constraints (cross-links, entanglements, etc.). We describe herein the results of recent work on model end-linked poly(dimethylsiloxane) networks where mesoscale computational studies were used to calculate elastic moduli using the NMR-derived molecular weight distributions as their sole input. These results are then compared to dynamic mechanical analysis measurements to assess the degree to which this new methodology can predict the mechanical properties of these simple elastomers. The results of this initial study suggest a high confidence in prediction and portend a nondestructive methodology capable of monitoring subtle changes in network structural motifs associated with material performance and age.

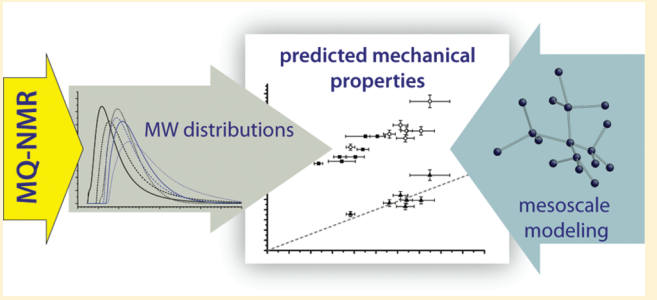

1. INTRODUCTION

Due in no small part to the versatile cross-linking chemistry available, over the last 50 years significant investment has been made in the research and development of specialized, highly tailored poly(dimethylsiloxane)- (PDMS-) based materials with ever increasing complex network structures. Creating an elastomeric network with specified material properties can be an Edisonian trial and error task, and there has been much effort spent to determine the structural motifs that control and tune resultant properties. One key observation from much of this work is that the combination of the complex nature of the siloxane elastomeric composites with frequently complex analytical and modeling techniques often presents significant challenges in the attempt to correlate various data with specific material constituents or network structural motifs. That is, fillers, stabilizers, cross-linking, network architecture, etc. presumably all affect the overall analytical observation, yet it is often not well understood how and to what degree the complexity of the materials (some components of which may be completely unknown) obfuscates subsequent interpretation of the data. In response to the above complication, there is a recognized need to investigate the physical chemical behavior of simple, idealized materials in an effort to identify the analytical "origins of response." For example, the effects of filler, network modalities, parent chain length, etc. have been investigated to understand their separate effects on resultant material properties.[1−8]

Simultaneously, there has been considerable effort to probe the degree to which an actual ideal PDMS network can be realized in the laboratory. These materials have been then used to test various rubber elasticity theories, to determine the effects on various chemical constituents and curing chemistries on mechanical properties, and so forth. A large subset of this work has focused on the investigation of structure−property relationships of a variety of monomodal, bimodal, as well as more complex siloxane networks.[2,9−16] Significant gaps, however, still exist in the fundamental understanding of how basic microscopic physical and chemical details of elastomers govern and modify macroscopic material properties. In an effort to address directly these gaps, complex experimental and modeling tools are being developed to be used alongside more traditional swelling, mechanical, and rheological testing.

Recently, it has been shown that the use of multiple quantum nuclear magnetic resonance (MQ−NMR) can provide an intriguing level of insight into the structure−property relationships in elastomeric networks.[17,18] MQ−NMR is sensitive to motion of polymer chains under the influence of various topological constraints (cross-links, physical entanglements, filler adsorption, etc.), and these dynamics can be related directly in principle to effective dynamic chain lengths (*vide infra*). Furthermore, many of the macroscopic properties of engineering materials can be directly related to the mobility of chains comprising the elastomer network, and MQ−NMR data has been therefore used to

Received: August 20, 2011
Revised: September 14, 2011
Published: September 29, 2011

dx.doi.org/10.1021/ma2019039 | *Macromolecules* 2011, 44, 8106–8115

obtain quantitative insight into network changes due to swelling,[17,19,20] thermal treatment,[16] filler content,[1] and radiation exposure.[21,22] It remains poorly understood, however, the degree to which the NMR distributions reflect *actual* molecular weight (MW) distributions in these soft solids and how much the distributions obtained by MQ−NMR can be relied on to predict material properties such as elastic shear modulus.

Since it is difficult to derive a theory that can predict macroscopic stresses from microstructural deformations, many of the predictive constitutive equations are phenomenological or empirical in nature. Furthermore, the complexity of multimodal networks generally prohibits obtaining high fidelity results using molecular dynamics (MD) methods. In an effort to increase the amount of coarse-graining, as compared to previous MD simulations, we have developed a mesoscopic numerical model that incorporates some details of polymer identity and microstructure without resorting to computationally intensive MD calculations, while maintaining the functionality and predictability required for engineering applications. Similar physics-based models have appeared in the literature. Arruda and Boyce proposed an eight chain network model to reproduce the stress response of elastomers for several types of deformation.[23] Hanson developed a model for filled and unfilled polydimethylsiloxane (PDMS) by physically modeling a small fraction of the polymer chains in a given volume, where the polymer intrachain forces and polymer−filler forces were based on more detailed MD simulations.[24]

Here, we report a concerted application of solvent swelling, mechanical analysis, MQ−NMR, and mesoscale modeling to a narrow range of bimodal networks of PDMS. It is the goal of this study to enhance the current applicability of the MQ−NMR technique by comparing dynamic mechanical analysis (DMA) results with moduli derived from mesoscale modeling that uses the NMR-based MW distribution data as its sole input. The technique will also be discussed in terms of its limitations as revealed through the comparison of derived and experimentally determined elastic shear moduli.

2. EXPERIMENTAL SECTION

2.1. Materials. The model networks consisted of telechelic, hydroxy-terminated linear polydimethylsiloxane (PDMS−OH) of two different chain lengths. The difunctional chains were cross-linked using tetraethoxysilane (TEOS), a tetra-functional cross-linking agent, using tin(II) 2-ethylhexanoate as a catalyst. All chemicals were obtained from Sigma-Aldrich.

The sample matrix consisted of four monomodal samples and seven bimodal samples. The monomodal samples were comprised of chains with nominal M_n of 8.0, 9.4, 32, and 54 kg/mol. All the polymers were characterized using gel permeation chromatography (GPC) (Malvern, Worcestershire, U.K.) using THF as the mobile phase. The polymers used in the bimodal systems are characterized by number-average molecular weights, M_n, of 8.0 kDa and 132.6 kDa with polydispersities of 1.42 and 1.73, respectively. The nomenclature for the bimodal series goes as "VMP_*X*_*Y*," where *X* and *Y* are the mole percentages of 8.0 kDa and 132.6 kDa chains, respectively. Note that the range appears quite narrow (100% to 50% short chains with an emphasis above 80%), though the formations are based on mole fractions to highlight the effects of the 8.0 kDa chains on samples when compared on an "average" chain molecular weight basis. The percentage cyclic and other volatile species was determined to be small (<3%) for the base polymer materials using gravimetric techniques and is consistent with previous reports on linear PDMS materials.[25]

The networks were synthesized by thorough mechanical mixing of the appropriate amounts of precursor chains followed by a degassing cycle (a vacuum oven under reduced pressure) at 25 °C in a circular PTFE mold. A 10% excess of a stoichiometric amount of TEOS was then mixed into the reaction mixture followed by another degassing cycle. The mixture was then put over an ice bath while a small amount (typically 25−50 mg of tin) of catalyst in hexanes was added, stirred, then degassed again over ice to prevent premature cross-linking. When the mixture contained no more bubbles (introduced through the mixing process), it was taken off the ice bath, put in a vacuum oven, and cycled again under reduced pressure. The temperature was slowly increased to 55 °C over several hours to evaporate off the hexanes thereby preventing the trapping of bubbles in the curing material. Finally the temperature was increased to 70 °C and the network was left to cure overnight. In some cases, particularly those where the mole percent of 132.6 kDa chains is large, the samples were left to cure for 2−3 days to promote a full cure.

2.2. Swelling. Swelling of the samples was performed using a 5:6 v/v toluene/acetone mixture at 29.5 °C as the swelling medium. This provides a theta condition that allows for a more direct comparison of other systems studied previously.[26−29] Small samples (each weighing about 50 mg or less) were swollen for 48 h and weighed periodically to monitor the process. Gravimetric analysis was performed with a microbalance (Mettler Toledo, Columbus, OH) and three samples of each polymer were swollen to assess curing homogeneity. After measurement, the networks were unswollen gradually in methanol then dried in a vacuum oven overnight at 45 °C. The samples were measured again to calculate the fraction soluble material extracted during the swelling process.

2.3. Mechanical Analysis. Dynamic mechanical analysis (DMA) of the bimodal polymers was conducted using a TA Instruments ARES-LS2 rheometer (New Castle, DE). Dynamic frequency sweep tests were conducted over the range ω = 0.1−100 rad/s at 23 °C using a torsion rectangle test geometry. Samples were approximately 1.0 cm by 2.0 cm in size with a variable thickness which averaged ∼0.3 cm. A shear strain of 6% or 10% was used (depending on specimen thickness), which is within the linear viscoelastic region of the material based on initial dynamic strain sweep tests at ω = 100 rad/s.

2.4. NMR. MQ−NMR allows for the quantification of dipolar couplings originating between protons on polymer chains experiencing a variety of physical and chemical topological constraints, which prevent the complete motional averaging of the homonuclear (^{1}H−^{1}H) dipolar interaction. The parameter that quantifies this resultant dynamical scaling of the nominal dipolar coupling strength is called the *residual* dipolar coupling magnitude, D_{res}, and be expressed through

$$\frac{D_{res}}{D_{stat}} = \frac{3}{5}\frac{r^2}{N}\langle P_2(\cos\alpha)\rangle \quad (1)$$

which relates it mathematically to the number of effective statistical segments between constraints, *N*. In the above expression D_{stat} is the static dipolar coupling value (8.9 kHz when considering rapidly rotating methyl groups); r^2 (assumed herein to be unity) is the squared end-to-end vector normalized by its unperturbed, melt state value; and $\langle P_2(\cos\alpha)\rangle$ is the time-averaged second order Legendre polynomial of the cosine of α, the angle between the Si−C vector and the chain backbone. This term takes into account rapid, intrasegmental motions; and because the angle α is roughly 90°, the time average value is therefore generally taken to be $^1/_2$. The prefactor of $^3/_5$ arises from considering average segmental orientations over the end-to-end vector of an idealized chain.[30] Equation 1 expresses the anisotropy of the proton−proton dipolar interaction resulting by the nonzero correlation between semi-local segmental motion and the chain end-to-end vector.

The NMR experiments were performed on a Bruker Avance spectrometer operating with a proton Larmor frequency of 400.13 MHz. MQ

Table 1. Base Characteristics, Swelling Results, and Network Analysis of the Investigated PDMS Networks[a]

sample	mol % 8k	mass% 8k	$M_{n,eff}$ (kDa)	Q	XLD (mol/cm^3 × 10^3)	v_2	w_s	T_e	f_{avg}
VMP_100_0_1	100	100	8.0	3.48 (0.05)	0.12	0.318	0.002 (0.0005)	0.826	3.41
VMP_100_0_2	100	100	8.0	3.60 (0.07)	0.12	0.302	0.014 (0.001)	0.604	3.20
VMP_95_5	95	53.4	14.2	4.20 (0.01)	0.068	0.253	0.008 (0.0006)	0.686	3.27
VMP_90_10	90	35.2	20.5	4.65 (0.02)	0.047	0.228	0.011 (0.0006)	0.638	3.23
VMP_85_15	85	25.5	26.7	4.93 (0.45)	0.036	0.215	0.027 (0.001)	0.484	3.13
VMP_80_20	80	19.4	32.9	5.49 (0.08)	0.029	0.192	0.015 (0.0007)	0.592	3.19
VMP_50_50	50	5.7	70.3	7.46 (0.41)	0.014	0.140	0.013 (0.0008)	0.616	3.21
M_8.0k	--	--	8.0	3.27 (0.09)	0.12	0.328	--	--	--
M_9.4k	--	--	9.4	3.67 (0.09)	0.10	0.290	--	--	--
M_32k	--	--	32.0	4.82 (0.05)	0.030	0.219	--	--	--
M_54k	--	--	54.0	6.45 (0.09)	0.018	0.163	--	--	--

[a] Effective number-average molecular weight ($M_{n,eff}$), swelling ratio (Q), mean cross-link density (XLD) determined from $M_{n,eff}$, measured volume fraction polymer in swollen gel (v_2), weight fraction extractable sol corrected for inert components (w_s), trapping factor (T_e), and average cross-link functionality (f_{avg}) calculated from eq 7. Error on experimental Q given in parentheses.

build-ups were measured using the method described by Saalwächter et al. with a pulse sequence designed to excite even-quantum coherences.[31] The resulting normalized build-ups were fit in a model-free way with the Tikhonov regularization package, FTIKREG, using the kernel function introduced in Chinn et al.[18] and covered in detail in Chassé et al.[32]

$$I_{nDQ}(\tau_{DQ}, D_{res}) = 0.5(1 - \exp[-(0.378 D_{res}\tau_{DQ})^{1.5}] \cos[0.583 D_{res}\tau_{DQ}]) \quad (2)$$

In these experiments 90° pulse lengths of $\tau_p = 3.3\ \mu$s and a recycle delay of 5 s were used. Here, 40−50 time points (τ_{DQ}) were chosen to measure the MQ build-up curve with more points chosen at early times to increase the confidence in the results from regularization.

2.5. Modeling. To compare with experiments and to explore how the structural motif contributes to the material strength, we employ a coarse-grained, mesoscopic polymer network model previously applied to radiation-induced aging of a filled PDMS material.[33] This "vertex" model consists of a set of cross-link nodes (beads) connected via a single finite extensible nonlinear elastic (FENE) potential,

$$V_{FENE}(r) = -\frac{1}{2} k R_0^2 \ln\left[1 - \left(\frac{r}{R_0}\right)^2\right], \quad r < R_0 \quad (3)$$

which represents the chains (springs) between cross-links. In the above equation k is the spring constant and R_0 is the maximum extension of the FENE bond. In addition, there is a repulsive Lennard-Jones interaction between all cross-link positions to simulate excluded volume effects,

$$\begin{aligned} V_{LJ}(r) &= 4\varepsilon\left[\left(\frac{\sigma}{r}\right)^{12} - \left(\frac{\sigma}{r}\right)^{6} + \frac{1}{4}\right], & r \le 2^{1/6}\sigma \\ &= 0, & r > 2^{1/6}\sigma \end{aligned} \quad (4)$$

where ε is the energy scale of the potential and σ is the diameter of a sphere that represents the cross-link.[34]

The network was generated by randomly placing cross-link nodes within the computational domain by sampling from the MW distributions measured with MQ−NMR. The cross-links were then connected by inserting FENE bonds, such that each node was tetra-functional. The FENE bond length, l, was computed using the mean squared end-to-end distance for an ideal chain in a network

$$l = \sqrt{\langle R^2 \rangle} = \sqrt{\frac{MW_{chain} b^2}{MW_{monomer} N_k}} \quad (5)$$

where b is the Kuhn length and N_k is the number of monomers in a Kuhn length. Assuming an entropic spring, the spring constant can be expressed as $k = 3k_BT/l^2$. Also, the cross-link density in the model was consistent with the average density computed from these distributions. Once complete, we relax the system to equilibrium and check the resulting bond distribution to verify it has not deviated from the original NMR data.

To compute the shear modulus, we apply a sequence of small strain uniaxial deformation steps ($\lambda = (\Delta L)/(L) = 1.00675$) followed by an energy minimization step and then calculate the slope of the resulting stress response. Note that dynamics are completely removed from the system by using the energy minimization between each deformation. These calculations were performed using custom software to prepare the networks, and the LAMMPS molecular dynamics simulator to model the deformation and compute the stresses.[35] Despite its simplicity, the model can reproduce nonlinear elastic behavior as well as predict the permanent set of an irradiated material under strain.[33]

3. RESULTS AND DISCUSSION

3.1. Network Ideality: Swelling. Equilibrium solvent swelling was employed to investigate the molecular structure of the "model" networks. Considerable effort over the last 40 years has sought to probe to degree to which an actual ideal PDMS network can be realized in the laboratory. Here, swelling serves to assess the similarity of the current materials to those investigated previously. More importantly, the results are also used to quantify the various network nonidealities inherent in these materials and correct for them in regards to the mechanical and computational data.

The measured swelling ratio, Q, is given in Table 1. Comparing these values against those for similar networks[26−29] (also swollen under approximate theta conditions) demonstrates that despite different workers, chemistries, and starting materials, our materials compare well with others investigated previously. The work of Patel and co-workers[8] represents the only exception to the observation, and this difference is attributed to a significant excess of cross-linking agent used to synthesize the sample matrix. In that study, each sample synthesis was "optimized" based on the minimal degree of swelling (i.e., maximum equilibrium polymer volume fraction, v_2). This procedure resulted in significantly higher cross-linker to polymer ratios, r, typically around 1.7, whereas for the current work, the networks were made with a

dx.doi.org/10.1021/ma2019039 |Macromolecules 2011, 44, 8106–8115

Table 2. Elastic and Reduced Moduli from Dynamic Mechanical Analysis, G_{mech}, and Mesoscale Simulation, G_{mod} and G_{pre} [a]

sample	G_{mech} (MPa)	G_{mech}/RT (mol/m^3)	G_{mod} (MPa)	G_{mod}/RT (mol/m^3)	G_{pre}/RT (mol/m^3)	prefactor
VMP_100_0_1	0.251 (0.006)	101.3 (6.8)	1.37 (0.050)	553 (20)	63.9 (5.0)[b]	0.388
VMP_100_0_2	0.224 (0.028)	90.4 (18.3)	1.37 (0.050)	553 (20)	63.9 (5.0)[b]	0.388
VMP_95_5	0.218 (0.006)	88.0 (5.4)	1.04 (0.045)	420 (15)	48.6 (3.6)	0.385
VMP_90_10	0.201 (0.018)	81.1 (8.1)	0.850 (0.030)	343 (13)	39.9 (2.9)	0.387
VMP_85_15	0.170 (0.024)	68.6 (12.4)	0.737 (0.025)	297 (11)	34.6 (3.0)	0.395
VMP_80_20	0.165 (0.014)	66.6 (5.5)	0.852 (0.024)	343 (15)	39.7 (5.2)	0.385
VMP_50_50	0.117 (0.005)	47.2 (4.0)	0.679 (0.024)	274 (10)	30.7 (2.9)	0.383
VMP_50_50 (truncated)	--	--	0.652 (0.030)	263 (10)	--	--
VMP_50_50 (delta function)	--	--	0.682 (0.032)	275 (12)	--	--

[a] Error given in parentheses. [b] k and σ were determined so that prefactor was ca. 0.38 for VMP_100_0 material. Bimodal samples were then simulated with these values and a prefactor determined postsimulation.

constant ratio of 1.1 (10% excess) in order to compare them more directly with the majority of previously investigated materials.

A key component of this swelling study is the quantification of the soluble sol fraction present in these materials. Analysis of the fraction soluble material can provide direct information on many network characteristics such as elastically inactive chain defects, average junction functionality, etc. and yields parameters that are extremely sensitive to, for example, slight incompleteness in the end-linking process.[36,37] Following the branching theory formalism developed previously[36] we have calculated for the bimodal networks the various parameters that quantify the structure of an $A_4 + B_2$ network (that is, a difunctional polymer, B_2, reacted with a tetra-functional cross-linker, A_4). The results of this swelling analysis are tabulated in Table 1 and also include the equilibrium swelling degree, Q, and the fraction polymer in swollen gel, ν_2, for both the bimodal and monomodal networks. Also included are the fraction sol material, w_s, the trapping factor, T_e, and the average functionality of a cross-link, f_{avg} (*vide infra*). Note that w_s has been corrected for the 2.5 wt % unreactive (presumably cyclic oligomers) present in the starting PDMS melts and that it is reported to high accuracy due to the sensitivity of the microbalance to the small weight losses associated with the sol extraction. The weight percents extractable are all at or under 2.7 wt %, which is consistent with previous reports.[37,38] Also values for the trapping factors are all approximately 0.6 to 0.7 with exceptions for the VMP_100_0_1 and VMP_85_15 networks. This observed range is roughly consistent with those for end-linked PDMS networks that are made with slight stoichiometric imbalances ($r = 1.1-1.25$) of the cross-linker.[37−40]

The data in Table 1 can be used to, for example, to test various theories of rubber elasticity. Here we employ a common theory that takes into account both the effect of physical topological interactions (i.e., entanglements) and the effect of elastically active strands and junction points. It is based on the phantom network theory[41] and also takes into account the presence of an effective network of entanglements.[42] The modulus, G, under this theory can be expressed as

$$G = (\nu - \mu)k_B T + G_e T_e \quad (6)$$

where ν and μ are the concentrations of elastically active strands and junctions, respectively, T_e is the trapping factor, and G_e is the maximum contribution to the overall modulus due to trapped entanglements. G_e is typically taken to be G_N^0, the modulus of the rubbery plateau of a polymer melt above the entanglement molecular weight (0.20−0.29 MPa for linear PDMS[43,44]). From eq 6 the trapping factor can be thought of as the fraction of entanglements that are trapped by the network (i.e., not relieved in the swelling process). It is clear then that as the extent of reaction approaches unity, the trapping factor should also approach unity, indicating a completely linked network. It is apparent from the values of T_e that these networks, in fact, deviate strongly from the descriptor of "ideal." These values (given in Table 1) will be therefore used to adjust the experimental and computational moduli discussed below to account for the effects of these network imperfections.

Further analysis of the swelling data can yield information on the average functionality of a cross-link. One can express f_{avg} through the concentrations of elastically active components:

$$f_{avg} = 2\nu/\mu \quad (7)$$

Use of eq 7 requires the calculation of both ν and μ, which can be done again through the branching theory used to calculate T_e. This method is preferable, for example, to the more commonly employed $\nu = \rho RT/M_n$ that assumes complete end-linking of monodisperse polymer chains. From Table 1 it can be seen that the average functionality of cross-links for the bimodal samples is significantly less than 4, the value expected from the reactants.

The deviation of T_e and f_{avg} from their expected values indicates that the networks are far from idealized systems. These materials are consistent, however, with much of the library of networks investigated previously. Ultimately, the quantification of the nonideality is all that is required for the current work, and references to this deviation will be made only when necessary. Because the detailed treatment presented above was not done on the monomodal samples, they will no longer be discussed.

3.2. Mechanical Testing. Table 2 provides the storage modulus, G_{mech} obtained from DMA of the bimodal materials. The values were taken by extrapolating G' data to zero frequency. Also included is the reduced modulus G_{mech}/RT expressed in mol/m^3. As expected, the modulus decreases with increasing effective molecular weight, $M_{n,eff}$, calculated from a weighted molar average of the parent chain masses. The modulus values have been reduced by both RT and the value of T_e determined experimentally for each sample. Linear regression of the data yields an intercept at 85 mol/m^3, a value consistent with the reported G_N^0 values given above (0.20 MPa/RT = 81 mol/m^3). These data will be considered in further detail when making comparisons to the computationally derived modulus predictions below.

3.3. Multiple Quantum NMR. Results from the regularization of the multiple quantum build-ups for the bimodal networks are shown in Figure 1. The residual dipolar couplings were converted into distributions of effective chain length, N, through the

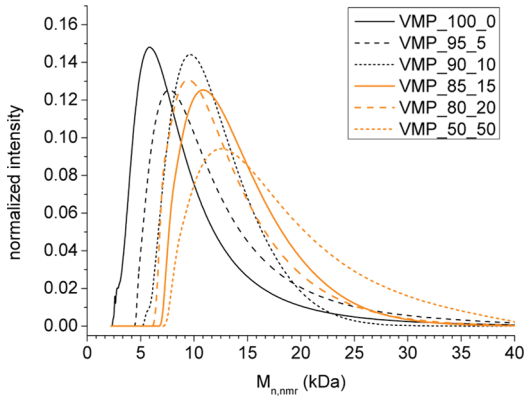

Figure 1. Normalized NMR-derived number-average molecular weight distributions (in kDa) for the bimodal series. The distribution for VMP_100_0 represents an average over those of the two samples synthesized.

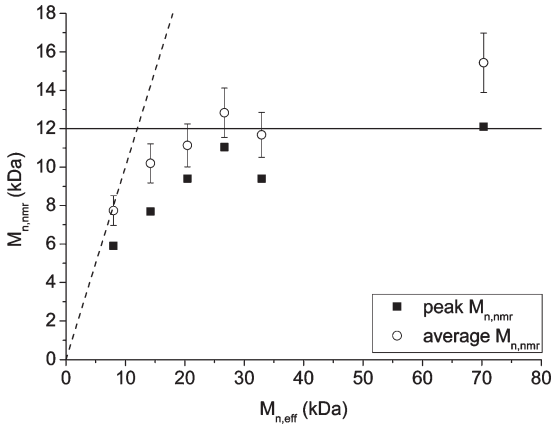

Figure 2. NMR-derived peak and average molecular weights, $M_{n,NMR}$, as a function of average molecular weight determined via GPC, $M_{n,eff}$. The solid line denotes the entanglement molecular weight, M_e = 12 kDa; and the dashed line is the 45° line. The error bars in the figure serve to approximate the confidence in the multiple quantum analysis procedure.

application of eq 1. Then these statistical lengths were converted into effective weight-average molecular weights by $M_{w,NMR} = NC_\infty MW_{monomer}$ where $MW_{monomer}$ = 74 g/mol is the dimethylsiloxane repeat unit molecular weight, and C_∞ = 6.43 is the characteristic ratio of PDMS (assumed herein to be in the large molecular weight limit).[45] Though it is strictly incorrect to assume that C_∞ represents the number of repeat units in a statistical segment,[46] it is a reasonable approximation for polymers with large backbone valence angles. It is important to note that this conversion process does not preserve relative areas under the population distributions due to the inverse dependence of D_{res} on N. Numerical correction is done after converting the data to molecular weight so that any given area between two given D_{res} values remains constant after conversion to $M_{w,NMR}$. This process is described in more detail in a previous publication.[22] After deriving the weight-average molecular weight distributions from the NMR data, the values where adjusted to rough *number-average* molecular weights by scaling by the value of the average polydispersity of the parent chain lengths which were both relatively low; 1.4 and 1.7 for the 8k and 132k chains, respectively. From this point forward, when molecular weights are discussed, they are understood to be number-averaged.

The general trend in the NMR data is a rightward shift in the distribution as the mole percent of 132.6 kDa chains increases. However, once this effective molecular weight (Table 1), surpasses the entanglement molecular weight for PDMS (M_e = 12 kDa) the distribution mean and peak value remain roughly constant. The distribution peak and mean molecular weights are shown in Figure 2. The 45° line has been drawn to highlight that the agreement between the GPC determined molecular weight and that from the NMR measurements is good. Above M_e, however, this agreement is poor but expected, as isothermal MQ−NMR as employed in this study is unable to distinguish between physical entanglements and chemical cross-links. Because entanglements represent the largest contribution to mechanical and viscoelastic properties for pure polymer networks with parent chain lengths well above M_e, one would expect the NMR response to plateau at this critical molecular weight as is indeed seen in Figure 2. As a final comment, there are several assumptions that go into converting the residual dipolar coupling into an effective molecular weight: the use of C_∞ as opposed to a molecular weight dependent C_n, the assumption that the end-to-end distance squared is Gaussian, and that motions about this end-to-end vector are ideal.[22,47,48] Despite these assumptions the NMR data is observed to behave roughly as expected:

$$M_{n,nmr} \approx M_n \text{ for } M_n < M_e \quad \approx M_e \text{ for } M_n > M_e \tag{8}$$

This observation increases the confidence in using the NMR data as a direct input into the modeling component discussed below.

As a final comment, it is interesting to note that in the case of these bimodal networks, the extracted distributions of the residual dipolar strength (and the effective chain length, Figure 1), much like the monomodal 8 kDa network, feature only a single, relatively narrow peak. At first glance, this might seem unexpected given the bimodality of the materials themselves. For the studied networks, however, there is most likely significant microscopic overlap (on the order of the average radius of gyration, R_g) between the 8 kDa and the 132 kDa chains, which presumably serves to homogenize the overall dynamics of the system. This homogenization has been discussed in detail previously[51] in terms of a significant restrictive effect of entanglements on the conformational space of individual chains. In addition, fluctuations of cross-links (which are neglected, for example, in affine network theories) and chain packing constraints (i.e., significant coopertivity effects) are understood to further homogenize local dynamic order parameters. We therefore conclude that it is not unreasonable for these materials to display a relatively homogeneous RDC response. Indeed, these data are consistent with previous observations for a chain molecular weight ratio of 20 (the present materials have a ratio of 16);[32] only for more disparate parent chain lengths (with a ratio on the order of 60) has a distinct bimodality in RDC been observed.[31]

3.4. Modeling and Analysis. The NMR-derived normalized molecular weight distributions plotted in Figure 1 are used to first construct an initial "cell" of polymer network. As stated in the methods section the cross-links were randomly placed through the simulation cell but their relative positions are consistent with the distributions from the NMR data as the selection criterion. This system of cross-links, which conforms to the cross-link density determined by NMR, is joined by FENE bonds and then

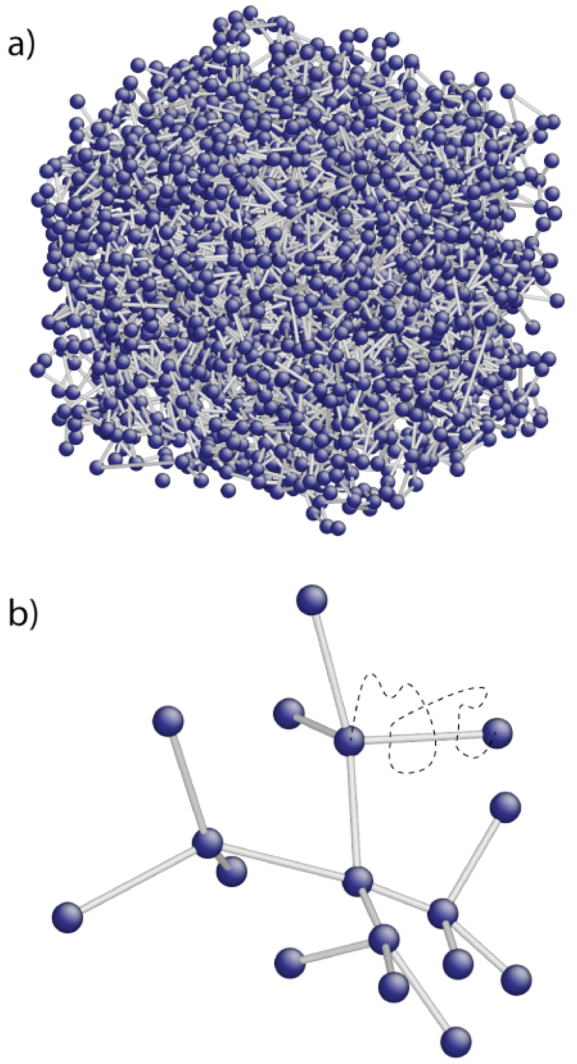

Figure 3. (a) Representation of typical bead−spring cell employed in the mesoscopic model approach. Cross-link junctions are represented schematically as beads connected through springs (straight bars) which serve as the polymer chains. For simplicity of the image, the bead radius has been chosen arbitrarily. (b) Breakout consisting of one central bead connected to nearest and next-nearest neighbors. The dashed line represents schematically the real chain that has been replaced by a single, effective entropic spring with $k = (3k_BT)/(\langle R^2 \rangle)$.

relaxed to equilibrium. This resultant network cell is then cross-checked against the original NMR molecular weight distribution to ensure that it remains consistent. An image of a representative simulated material using this mesoscopic model is shown in Figure 3.

The FENE potential is used to parametrize the elastic energy of the system, and the resulting modulus depends weakly on the value of l^2 chosen to calculate the spring constant, k, compared with the mean cross-link density of the network, which strongly affects the derived modulus values. This observation perhaps results from the fact that only a fraction of the bonds contribute to the stress experienced under deformation, and studies are currently underway by this group to investigate this phenomena in more detail.

Excluded volume interactions are parametrized through a standard Lennard-Jones potential to provide a balancing force

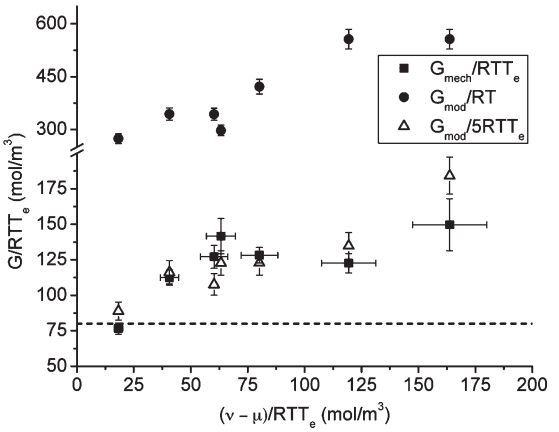

Figure 4. Simulation-derived, uncorrected reduced elastic moduli (black circles) against strand density determined from swelling experiments. Open triangles represent the simulation data scaled by both a factor of 5 and the experimental trapping factors. Mechanical data (black squares) overlaid for comparison. Error bars for swelling data only shown on G_{mech} data for clarity. Dashed line denotes $G_N^0/RT = 81$ mol/m^3.

to the compressive spring potential and to prevent neighboring chains from passing through another . The magnitude ε, was assigned a value of $k/30\sigma^2$, in accordance with more detailed molecular dynamics simulations of polymer systems[49] and the distance parameter, σ, was chosen to equal to the bond distance, l, to maintain the shape of the initial molecular weight distribution in the postequilibrium state.

The model networks experienced uniaxial strains of values up to 40%. The shear modulus was derived from the linear regression slopes of true stress vs true strain for data between 0 and 3% strain. The mechanical testing introduced strains up to 10%, but the computed modulus was insensitive to the inclusion of higher strains in the regression. The values of the storage modulus, G_{mod} from the bimodal networks are also tabulated in Table 2.

The values of G_{mod} derived from the uniaxial extension simulations are presented in Figure 4. Plotted for comparison is the DMA data, G_{mech}, given in Table 2. Some of these data have been divided by the trapping factor, T_e, to account for network imperfections due to incomplete end-linking. As with the mechanical testing results, the computationally determined reduced moduli, G_{mod}/RT, all lie above the value of the reduced plateau modulus, G_N^0/RT, as expected. Additionally, we have scaled the modeling data by a factor of 5 to bring it into approximate accord with those values determined via DMA. More comments on this seemingly arbitrary scaling factor will be given below.

Simulations were performed on the VMP_50_50 sample to quantify the dependence of the extracted G_{mod} values on the overall shape of the distribution. This sample was chosen due to its significant tail at $M_{n,NMR} > 12$ kDa. In addition to the NMR-derived distribution, also tested were a delta function at the nominal distribution mean and a truncated (and renormalized) distribution that replaces populations above M_e with a delta function (of appropriate area) at 12 kDa. Truncating the distribution in the tail does change the average molecular weight, but we fixed the value from the original distribution to isolate effects due to the shape of the profile. Though the majority of data in Table 2 were generated with networks with molecular weight distributions from NMR as the computational input, the

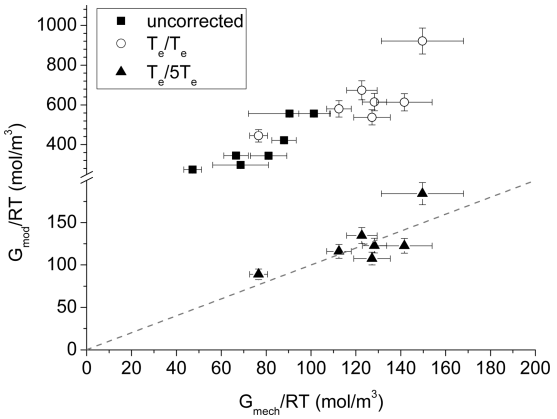

Figure 5. Direct comparison of reduced elastic moduli extracted from mechanical and computational analyses. Black squares represent the data without correction for network nonideality by the trapping factor, T_e. Open circles denote the corrected modulus values. The modeling moduli scaled by a factor of 5 (to bring them into accord with mechanical data, black triangles) are shown against the dashed gray, 45° line.

final G_{mod} values are effectively independent of the overall shape of the distribution. We believe this observation results because, like a mechanical measurement, storage moduli are determined as a bulk average and are therefore dominated by the average chain molecular weight dictated by the chemical and physical topological constraints imposed on the networks. Additionally, the parent chain molecular weights are large enough and the deformation strains small enough that issues of finite extensibility are assumed to be not an issue. The universality of this observation is not fully known, but for this range of bimodality under low strain, a modulus independent of MW distribution is not unreasonable. To address this knowledge gap, however, we are currently considering extremely bimodal networks (those with MW ratios greater than those currently investigated) and their associated behavior under both low and high strain conditions.

Finally, since the current goal of this work is to demonstrate the ability of NMR and modeling to predict the elastic modulus of an elastomeric network, Figure 5 correlates the computationally and experimentally derived moduli. Also, the effects of correcting for network nonideality (as expressed by the trapping factor, T_e) are also demonstrated, resulting in an upward shift in reduced moduli for both methods. Note that this simple T_e correction is not sufficient to bring into agreement the modeling and the DMA results. From the figure it is apparent that the reduced moduli values, G_{mod}, from the modeling results are overestimated by approximately a factor of 5.

The present NMR distributions cannot distinguish between entanglements and cross-links for chain lengths greater than the entanglement molecular weight, and the model used presently is subsequently forced to treat the constraints equivalently. In addition, because this basic model connects cross-link beads with springs that represent an *entire* chain, it is unable to generate explicitly the chain structures necessary for entanglement. In fact, the only place where chains statistics enter this model is when they are invoked in the calculation of the spring constant. Despite these factors, the modulus data from simulation are still in fairly good agreement with the mechanical tests.

A possible explanation for the disparity between simulation and experiment is the difference between the average cross-link functionalities of the real and virtual networks. Though the effective cross-link densities (including the contribution from entanglement "cross-links") are preserved in the model by use of the NMR distributions, there is nothing about the generation of the present model systems that insures agreement of functionalities, a variable expected to strongly influence overall mechanical properties of networks. For example, increasing the functionality of the cross-linking agent from 3 to 4 would expect to increase the modulus, for example, of a phantom network by a factor of 1.5 holding strand density (molecular weight) constant. Though swelling data indicates the mean functionality of the current networks is 3.2, the model networks have a higher value of 3.8, which is consistent with the larger modulus values derived from the model. This difference, however, amounts to only a factor of 1.51 and is therefore not large enough to account solely for the present disparity.

A suspect of larger consequence on the computed moduli is the equivalent treatment of chemical and physical constraints. Recall that the present NMR experiment is largely insensitive to the differences between chemical and physical constraints in the material. Therefore, the effects of entanglements and cross-links are both present in the data in Figure 2, and one cannot separate herein their individual contributions for input into this model. Modeling these distributions strictly as cross-linked systems (i.e., ignoring the fundamental differences between cross-links and entanglements), one would indeed expect an overestimation in the value of the elastic modulus. It has been shown both experimentally[8] and computationally[50] that roughly 2.2 entanglement lengths are needed to contribute to the modulus in the same way as one chemical cross-link. Within the framework of both the affine and phantom network models for rubber elasticity, one can attempt to estimate the effect on the modulus of modeling the entanglements as elastically active cross-links.

For an affine network, the elastic modulus is expressed by

$$G = \nu k_B T + G_e T_e \tag{9}$$

where we have explicitly accounted for the entanglement contribution as in eq 6. For the phantom network, eq 6 can be rewritten in terms of the average cross-link junction functionality

$$G = \nu k_B T\left(\frac{f-2}{2}\right) + G_e T_e \tag{10}$$

If we take the results mentioned above, replace G_e with $2.2\nu k_B T$, and use the average values for the trapping factor and functionality ($T_e = 0.635$; $f = 3.23$), we can calculate the degree to which $((G)/(T_e))$ is overestimated when considering both chemical and physical topological constraints as cross-links. At the phantom network and affine network limits: $G/T_e = 4.1\nu k_B T$ and $5.0\nu k_B T$, respectively. Taking ratios of these moduli to those obtained by considering only the network chain contributions to the modulus (i.e., the second right-hand terms in eq 9 and eq 10) yields a range of 3.2−6.8, which bounds the overestimation observed with the present model. In fact, the "average" overestimation is precisely 5, the effectively arbitrary factor used in Figures 4 and 5 to scale the simulation data.

Another approach to addressing this overestimation is to alter the value of a model parameter such that the calculated modulus values are agreement with the mechanical data. Under this strategy, k is fixed by invoking the idea of the entropic chain, and the bead diameter, σ, is held constant at the value of $(\langle R^2\rangle)^{1/2}$. The only remaining fundamental parameter, then, is ε, the energy scale of the potential that dictates the strength of repulsion

dx.doi.org/10.1021/ma2019039 |*Macromolecules* 2011, 44, 8106–8115

between beads. Traditionally, the value of ε has been fixed at $\sim k_BT$, but it is interesting to determine the value at which the modeling and experimental moduli are brought into accord. One would expect that to lower the modulus, the strength of bead−bead repulsion must necessarily decrease, indicating a "weaker" network from the perspective of interbead interactions. In previous work the value of k has been calculated as $30\varepsilon/\sigma^2$, where the factor of 30 is chosen to provide a balance between bead repulsion and the spring constant, effectively preventing chains crossing through one another.[50] Under the current considerations, the parameters k, ε, and σ are all being adjusted independently of one another, and this action is therefore equivalent to changing the factor, 30. For these comparative simulations, the value of ε has been chosen so that the prefactor for the modulus under the phantom network model, $(f-2)/f$, is the value calculated from the experiments. As the average functionality ($f = 3.23$) is roughly constant for all the networks synthesized, this prefactor is set at 0.38.

To do this within the simulations, the values of both k and ε were adjusted so that the simulation yielded the appropriate prefactor, 0.38. This process was done for the 8 kDa monomodal sample only, and the resultant values were used for the remainder of the (bimodal) systems to ensure that they could independently generate simulations with a consistent value for this prefactor. To produce the proper values, both k and ε had to be reduced such that $k \sim k_BT/\sigma^2$ and $\varepsilon \sim \sigma^2/300$. A reduction in ε alone, indicating a more weakly repulsive system, was not enough to modify the prefactor to the desired level. Only when the spring constant was modified in tandem were we able to reduce the value to 0.38. For the systems studied, only a single value each for the two parameters was sufficient, demonstrating the consistency between simulations and a strong linear response to increases in cross-link density. The moduli, G_{pre}, and prefactors extracted from these simulations are given in Table 2 and reveal an underestimation in the elastic modulus for the entire series of materials. This observation is not unexpected as these simulations consider a phantom network-like system where the effects of entanglement and excluded volume are not explicitly modeled. It is promising, however, that these results along with those from the simulations considered above *bound* the experimental data. Though it is difficult in this simple model to ascribe a physical quantity to the value of the strength of the Lennard-Jones potential, one can tune the value of the energy scale so that the extracted moduli from the simulations represents well those measured experimentally. For the present samples, the values of σ and k that accomplish this are given by $3k_BT/800$ and $3k_BT/2\sigma^2$, respectively.

Since NMR is used as the sole input for the creation of the polymer network cell using in the mesoscale modeling, the MQ data must also be considered to explain the discrepancy between the modeling results and the experiments. The conversion of residual dipolar couplings to molecular weight requires various assumptions, many of which were mentioned above. The simplest approximation to address is the assumption that the value of C_∞ applied to any network regardless of the molecular weight of the parent chain. The use of C_∞ as opposed to C_n might be expected to cause overestimations in the molecular weight values (and hence average and peak masses) particularly at low average molecular weights like the VMP_100_0 samples. Molecular dynamics simulations, however, have shown[45] that for PDMS chains above ca. 4000 Da the value of C_n does not differ markedly from C_∞. For example, use of C_n in molecular weight calculations would result in masses differing by only a factor of $C_n/C_\infty = 0.94$.

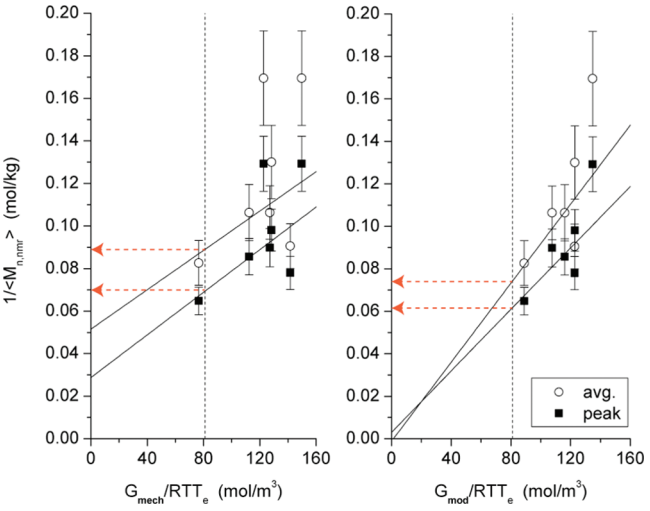

Figure 6. Inverse NMR molecular weights (open circle = average, closed square = peak) against mechanically (left) and computationally (right) determined reduced moduli. Vertical dashed line represents the plateau modulus, $G_N^0/RT = 81$ mol/m^3. Solid lines are linear regression results for all four sets of data. The red dashed arrows denote where the regression lines intersect the plateau modulus line and indicate an estimate of the inverse entanglement molecular weight. The linear regression procedure incorporates explicitly the error bars given in the figure.

Other, more complex assumptions made when processing the NMR data may also affect the computational predictions. The local quantities observed by NMR must be extended, in some sense, to quantities that reflect the long-range, connective nature of a linear polymer chain. Specifically, the NMR observable, which ideally reflects only local two-body dipolar interactions (between, e.g., protons within a single dimethylsiloxane monomer), is strongly affected by concerted, long-range chain motions. To directly relate, then, local to global dipolar coupling measurements, one must take into account formally some notion of chain conformational statistics, dynamical modes, etc. This is generally done by assuming chains behave ideally and can be therefore be described by basic conformational models. These treatments generate effective scaling factors by which the static dipolar interactions are reduced, with each factor relating to a different motion being averaged over (for example, an average *about* the backbone or an average *over the contour* of the backbone).[47] Choosing an inappropriate or incomplete description of chain conformation would be expected to generate erroneous scaling factors, and therefore values for N and $M_{n,NMR}$ would subsequently be suspect as well. Nevertheless, it is promising that the modulus values predicted by simulation using NMR data as the only input are within an order of magnitude with those derived experimentally. On-going research by the current group aims to refine the present mesoscopic model by including, for example, modeling individual chains as multibead−spring entities, which allows for the explicit consideration of the role of entanglement in these simulations. In addition, alternative model networks differing in network architecture, structural motif, etc. are being synthesized to probe in more detail the fundamental limits and applicability of this methodology.

Despite the ultimate discrepancy between the raw simulation data and the mechanical analysis as discussed in detail above for this preliminary research, it is important in the end to recognize

that both the model and the experimental work can reproduce several physically meaningful values not directly measured or calculated. Figure 6 considers the inverse of the average and peak NMR molecular weights (see Figure 2) against the reduced moduli from DMA (left panel) and simulation (right panel). Given in the figure also are linear regressions of the four data sets shown as solid lines. To put confidence in these modulus values, one would expect that the intersection of these lines with the melt plateau modulus (given as the vertical dashed line) should give a reasonable estimate of the critical molecular weight for entanglement. This result is expected since $G = G_0^N \propto (\rho RT)/(M_e)$. For the four values considered presently the values of M_e (determined through the combined NMR/modulus measurement) range between 11.2 and 16.2 kDa, in reasonable agreement with the accepted value of 12 kDa.

Recalling that under the affine network model, the elastic modulus can be expressed as $G = \rho RT/M_s$, where ρ is the mass density and M_s is an effective strand molecular weight. If the modeling results are internally consistent, then the slope of the regressed data should simply be the inverse of the density (i.e., specific weight). From the extracted values for the slopes of the simulation-derived moduli (right panel), the density of the material ranges from 1.1−1.3 g/cm,^{3} a reasonable range compared to the experimental value of 0.96 g/cm^3. The fact that the intercepts are roughly zero for the regressed simulation data reflects the fact that the simulation conditions correspond to those of ideal networks where structural imperfections (loops, dangling ends, etc.) are not generated, vis-à-vis the synthesized bimodal networks. Only for the real systems (as measured by DMA) do nonzero intercepts exist, though because of the nonideal character of these "model" networks, we refrain from making serious comment about the physical meaningfulness of the slopes and intercepts. Ultimately, however, these data do exhibit some expected behavior, and we merely highlight this fact to offer additional support to the validity of the current technique.

4. CONCLUSIONS

Herein we describe the application of multiple quantum NMR experiments to the prediction of siloxane network elastic moduli using a mesoscale computational modeling approach. Using only a few polymer specific quantities (characteristic ratio, monomer molecular weight, etc.) and invoking basic polymer physics concepts, we are able to reasonably predict a practical mechanical property with NMR data as the model's only input. Issues in faithfully reproducing mechanical analysis data were discussed in terms of treating entanglements and cross-links equivalently, disparities in average cross-link functionality, Leonard-Jones energy scales, and NMR data analysis. Realistically, a combination of several of the approximations discussed above are likely to account for the observed discrepancy, but from a practical perspective, the results from the present model bimodal networks can serve as a training set that will enable us to further test this methodology on more complex networks such as bimodal networks with extremely short chain lengths,[2,9] silica-reinforced filled networks, and engineering materials that have been investigated by this group in detail previously. We anticipate that this potentially nondestructive, noninvasive methodology can also be applied in a straightforward fashion to, for example, in situ monitoring of subtle aging mechanisms or the effects of material usage in harsh environments.

AUTHOR INFORMATION

Corresponding Author
*E-mail: mayer22@llnl.gov.

ACKNOWLEDGMENT

This work was performed under the auspices of the U.S. Department of Energy by Lawrence Livermore National Laboratory under Contract DE-AC52-07NA27344.

REFERENCES

(1) Papon, A.; Saalwachter, K.; Schaler, K.; Guy, L.; Lequeux, F.; Montes, H. *Macromolecules* **2011**, *44* (4), 913–922.
(2) Llorente, M. A.; Andrady, A. L.; Mark, J. E. *J. Polym. Sci., Polym. Phys.* **1981**, *19* (4), 621–630.
(3) Llorente, M. A.; Andrady, A. L.; Mark, J. E. *Colloid Polym. Sci.* **1981**, *259* (11), 1056–1061.
(4) Aranguren, M. I.; Mora, E.; Degroot, J. V.; Macosko, C. W. *J. Rheol.* **1992**, *36* (6), 1165–1182.
(5) Cohenaddad, J. P.; Ebengou, R. *Polymer* **1992**, *33* (2), 379–383.
(6) Cohenaddad, J. P. *Polymer* **1989**, *30* (10), 1820–1823.
(7) Aranguren, M. I.; Mora, E.; Macosko, C. W. *J. Colloid Interface Sci.* **1997**, *195* (2), 329–337.
(8) Patel, S. K.; Malone, S.; Cohen, C.; Gillmor, J. R.; Colby, R. H. *Macromolecules* **1992**, *25* (20), 5241–5251.
(9) Andrady, A. L.; Llorente, M. A.; Mark, J. E. *J. Chem. Phys.* **1980**, *72* (4), 2282–2290.
(10) Maiti, A.; Gee, R. H.; Weisgraber, T.; Chinn, S.; Maxwell, R. S. *Polym. Degrad. Stab.* **2008**, *93* (12), 2226–2229.
(11) Wen, J. A.; Mark, J. E. *J. Appl. Polym. Sci.* **1995**, *58* (7), 1135–1145.
(12) Shim, S. E.; Isayev, A. I. *Rheol. Acta* **2004**, *43* (2), 127–136.
(13) Gee, R. H.; Maxwell, R. S.; Balazs, B. *Polymer* **2004**, *45* (11), 3885–3891.
(14) Charlesby, A. *Proc. R. Soc. London A* **1955**, *230* (1880), 120–132.
(15) Cochrane, H.; Lin, C. S. *Rubber Chem. Technol.* **1993**, *66* (1), 48–60.
(16) Giuliani, J. R.; Gjersing, E. L.; Chinn, S. C.; Jones, T. V.; Wilson, T. S.; Alviso, C. T.; Herberg, J. L.; Pearson, M. A.; Maxwell, R. S. *J. Phys. Chem. B* **2007**, *111*, 12977–12984.
(17) Saalwächter, K. *Prog. NMR Spectrosc.* **2007**, *51*, 1–35.
(18) Chinn, S. C.; Alviso, C. T.; Berman, E. S. F.; Harvey, C. A.; Maxwell, R. S.; Wilson, T. S.; Cohenour, R.; Saalwächter, K.; Chassé, W. *J. Phys. Chem. B* **2010**, *114* (30), 9729–9736.
(19) Cohenaddad, J. P.; Domard, M.; Herz, J. *J. Chem. Phys.* **1982**, *76* (5), 2744–2753.
(20) Cohenaddad, J. P.; Domard, M.; Lorentz, G.; Herz, J. *J. Phys.-Paris* **1984**, *45* (3), 575–586.
(21) Maiti, A.; Weisgraber, T.; Dinh, L. N.; Gee, R. H.; Wilson, T.; Chinn, S.; Maxwell, R. S. *Phys. Rev. E* 2011, *83* (3), -.
(22) Dinh, L. N.; Mayer, B. P.; Maiti, A.; Chinn, S. C.; Maxwell, R. S. *J. Appl. Phys.* **2011**, *109*, 094905.
(23) Arruda, E. M.; Boyce, M. C. *J. Mech. Phys. Solids* **1993**, *41* (2), 389–412.
(24) Hanson, D. E. *Polymer* **2004**, *45* (3), 1055–1062.
(25) Gottlieb, M.; Macosko, C. W.; Benjamin, G. S.; Meyers, K. O.; Merrill, E. W. *Macromolecules* **1981**, *14* (4), 1039–1046.
(26) Clarson, S. J.; Galiatsatos, V.; Mark, J. E. *Macromolecules* **1990**, *23* (5), 1504–1507.
(27) Cohen, C.; Yoo, S. H.; Hui, C. Y. *Polymer* **2006**, *47* (17), 6226–6235.
(28) Sivasailam, K.; Cohen, C. *J. Rheol.* **2000**, *44* (4), 897–915.
(29) Sukumaran, S. K.; Beaucage, G.; Mark, J. E.; Viers, B. *Euro. Phys. J. E* **2005**, *18* (1), 29–36.
(30) Sotta, P.; Deloche, B. *Macromolecules* **1990**, *23* (7), 1999–2007.

(31) Saalwächter, K.; Ziegler, P.; Spyckerelle, O.; Haider, H.; Vidal, A.; Sommer, J.-U. *J. Chem. Phys.* **2003**, *119*, 3468–3482.
(32) Chassé, W.; Valentin, J. L.; Genesky, G. D.; Cohen, C.; Saalwächter, K. *J. Chem. Phys.* **2011**, *134* (4), No. in press.
(33) Weisgraber, T. H.; Gee, R. H.; Maiti, A.; Clague, D. S.; Chinn, S.; Maxwell, R. S. *Polymer* **2009**, *50* (23), 5613–5617.
(34) Grest, G. S.; Kremer, K. *Phys. Rev. A* **1986**, *33* (5), 3628–3631.
(35) Plimpton, S. *J. Comput. Phys.* **1995**, *117* (1), 1–19.
(36) Miller, D. R.; Macosko, C. W. *Macromolecules* **1976**, *9* (2), 206–211.
(37) Valles, E. M.; Macosko, C. W. *Macromolecules* **1979**, *12* (4), 673–679.
(38) Llorente, M. A.; Mark, J. E. *Macromolecules* **1980**, *13* (3), 681–685.
(39) Meyers, K. O.; Bye, M. L.; Merrill, E. W. *Macromolecules* **1980**, *13* (5), 1045–1053.
(40) Granick, S.; Pedersen, S.; Nelb, G. W.; Ferry, J. D.; Macosko, C. W. *J. Polym. Sci., Polym. Phys.* **1981**, *19* (11), 1745–1757.
(41) Flory, P. J.; Gordon, M.; McCrum, N. G. *Proc. R. Soc. London A.* **1976**, *351* (1666), 351–380.
(42) Graessley, W. W. *Macromolecules* **1975**, *8* (2), 186–190.
(43) Langley, N. R. *Macromolecules* **1968**, *1* (4), 348–352.
(44) Langley, N. R.; Ferry, J. D. *Macromolecules* **1968**, *1* (4), 353–358.
(45) Neuburger, N.; Bahar, I.; Mattice, W. L. *Macromolecules* **1992**, *25* (9), 2447–2454.
(46) Flory, P. J., *Principles of Polymer Chemistry*. Cornell University Press: Ithaca, NY, 1953.
(47) Sotta, P.; Deloche, B. *Macromolecules* **1990**, *23* (7), 1999.
(48) Mayer, B. P.; Chinn, S. C.; Maxwell, R. S.; Reimer, J. A. *Chem. Eng. Sci.* **2009**, *64* (22), 4684–4692.
(49) Kremer, K.; Grest, G. S. *J. Chem. Phys.* **1990**, *92* (8), 5057–5086.
(50) Duering, E. R.; Kremer, K.; Grest, G. S. *J. Chem. Phys.* **1994**, *101* (9), 8169–8192.
(51) Saalwächter, K.; Sommer, J.-U. *Macromol. Rapid Commun.* **2007**, *28* (14), 1455–1465.